



Cold-Formed Steel Lipped Channel Section Columns Undergoing Local-Overall Buckling Interaction

Krishanu Roy¹ · Tina Chui Huon Ting² · Hieng Ho Lau³ · Rehan Masood^{1,6} · Rayed Alyousef⁴ · Hisham Alabduljabbar⁴ · Abdulaziz Alaskar⁵ · Fahed Alrshoudi⁵ · James B. P. Lim¹

Received: 7 February 2020 / Accepted: 10 December 2020 / Published online: 6 January 2021
© Korean Society of Steel Construction 2021

Abstract

This paper presents an experimental and finite element (FE) investigation into the local-overall buckling interaction behaviour of axially loaded cold-formed steel (CFS) channel section columns. Current design guidelines from the American Iron and Steel Institute (AISI) and the Australian and New Zealand Standards (AS/NZS) recommend the use of a non-dimensional strength curve for determining the axial capacity of such CFS channel section columns. This study has reviewed the accuracy of the current AISI (2016), AS/NZS (2018) and Eurocode (EN 1993-1-3) design guidelines for determining the axial capacity of CFS channel sections under local-overall buckling interaction failure. A total of 40 tests were conducted on CFS channel sections covering stub, short, intermediate, and slender columns with varying thicknesses. A nonlinear FE model was then developed and validated against the test results. The validated FE model was used to conduct a parametric study comprising 70 FE models to review the accuracy of the current design guidelines in accordance with AISI (2016), AS/NZS (2018) and Eurocode (EN 1993-1-3). It was found that the AISI (2016) and AS/NZS (2018) are conservative by 10 to 15% on average when determining the axial capacity of pin-ended CFS channel section columns undergoing local-overall buckling interaction. Eurocode (EN 1993-1-3) design rules were found to lead to considerably more conservative predictions of column axial load capacity for CFS channels. This paper has therefore proposed modifications to the current design rules of AISI (2016) and AS/NZS (2018). The accuracy of proposed design rules was verified using the FE analysis and test results of CFS channel section columns undergoing local-overall buckling interaction.

Keywords Buckling interaction · Cold-formed steel · Compression member · Finite element analysis · Local-overall buckling interaction

✉ Krishanu Roy
kroy405@aucklanduni.ac.nz

Tina Chui Huon Ting
tina.ting@curtin.edu.my

Hieng Ho Lau
HHLau@swinburne.edu.my

Rehan Masood
rmas769@aucklanduni.ac.nz

Rayed Alyousef
r.alyousef@psau.edu.sa

Hisham Alabduljabbar
h.alabduljabbar@psau.edu.sa

Abdulaziz Alaskar
abalaskar@ksu.edu.sa

Fahed Alrshoudi
falsrshoudi@ksu.edu.sa

James B. P. Lim
james.lim@auckland.ac.nz

- ¹ Department of Civil and Environmental Engineering, The University of Auckland, Building 906, Level 4, Room 413, Newmarket campus, Auckland 1010, New Zealand
- ² School of Engineering and Science, Curtin University Sarawak, Miri, Sarawak, Malaysia
- ³ Faculty of Engineering, Computing and Science, Swinburne University of Technology, Kuching, Sarawak, Malaysia
- ⁴ Department of Civil Engineering, College of Engineering, Prince Sattam Bin Abdulaziz University, Al-kharj 11942, Saudi Arabia
- ⁵ Department of Civil Engineering, College of Engineering, King Saud University, Riyadh 11362, Saudi Arabia
- ⁶ Department of Construction Engineering and Management, National University of Sciences and Technology, Islamabad, Pakistan

List of Symbols

A	Overall web length of section
A_e	Effective area of the section
B	Overall flange width of section
C	Overall lip width of section
COV	Coefficient of variation
C_p	Correction factor depending on the number of tests
E	Young's modulus of elasticity
FEA	Finite element analysis
F_m	Mean of variation of the fabrication factor
F_n	Critical buckling stress
F_y	Yield load
i	Radius of gyration
M_m	Mean of variation of the material factor
P_{EN}	Axial strength
P_{AISI}	Axial capacity obtained from American Iron and Steel Institute
P_{EXP}	Axial capacity obtained from experiments
P_{FEA}	Axial capacity obtained from finite element analysis
P_m	Mean value of the tested to predicted load ratio
L_{cr}	Plane buckling length
N_{cr}	Elastic critical force
V_f	Coefficient of variation of the fabrication factor
V_m	Coefficient of variation of the material factor
V_p	Coefficient of variation of the tested to predicted load ratio
V_q	Coefficient of variation of the load effect
β_0	Target reliability index
$\sigma_{0.2}$	Static 0.2% proof stress;
λ	Imperfection factor
λ_c	Non dimensional slenderness ratio
χ	Reduction factor for the relevant buckling mode
ϕ	Capacity reduction factor

1 Introduction

Cold-formed steel (CFS) channel sections have been considered a viable alternative to hot rolled steel channels because of their superior strength to weight ratio and ease of fabrication. These channel sections are used widely in CFS building components. Despite the popularity of CFS channel sections, these remain susceptible to local, distortional, flexural, and flexural–torsional buckling failures (Loughlan and Yidris 2014; Hancock et al. 1994; Wang et al. 2016; Zhang et al. 2007; Young and Hancock 2003).

Buckling behaviour of CFS channel sections has been studied extensively in the last two decades, with focus on code conservativeness. Heva et al. (2012) conducted compression tests on CFS channel sections under flexural–torsional buckling at both ambient and elevated temperatures and showed that Australia-New Zealand standard (AS/NZS

4600) design guidelines were conservative when predicting the axial capacity of CFS channels. On the other hand, Kandasamy et al. (2016) provided the optimum size of lip considering the flexural–torsional buckling interaction for CFS channel beams under restrained boundary conditions. Martins et al. (2015) have presented a critical review on the non-linear behavior and design of CFS columns under local-distortional buckling interaction. Other work in the area includes Gunalan and Mahendran (2013), who investigated the axial capacity of fixed ended CFS channel section columns subjected to flexural–torsional buckling interaction. This study showed how current design guidelines by the American Iron and Steel Institute and Australia-New Zealand standards (AS/NZS 4600) are over-conservative. Most recently, Ye et al. (2018) reported an experimental investigation on local-flexural interactive buckling behaviour of CFS channel section columns. Here, a total of 36 axial compression tests on CFS channel sections of three different lengths (1 m, 1.5 m and 2 m) and four different cross-sections were conducted under pin-ended boundary conditions (Ye et al. 2018).

Interaction between local, distortional, and overall buckling modes plays an important role in determining the section capacities of CFS channel sections under axial compression. However, very limited research is available in the literature for understanding the effect of buckling interactions on the axial capacity of CFS channels. Santos et al. (2012) conducted experimental tests on lipped channels undergoing local-distortional-global buckling interactions. Their study showed that the intermediate columns are susceptible to buckling interactions (Santos et al. 2012).

The Direct Strength Method (DSM) includes the effect of buckling interactions. However, the DSM does not have provisions to include the shift of effective centroid when compressive force is applied to pin-ended columns. Young (2004, 2005, 2006) and Rhodes and Harvey (1977) explained that the shift of effective centroid is caused by the asymmetric redistribution of longitudinal stress due to local buckling. This leads to an eccentricity of the applied load in pin-ended columns.

In terms of CFS angle section columns, significant research is available in the literature. Popovic et al. (1999) investigated the compression capacity of CFS steel angle section columns. In their tests, the primary failure mode for most of the angle sections was overall buckling and flexural–torsional buckling. It was concluded that the Australia-New Zealand standard (AS/NZS 4600) design guidelines were conservative for shorter columns but un-conservative for slender columns (Popovic et al. 1999). Young (2004, 2005) performed experimental tests on angle section columns and showed that the Australia-New Zealand standard (AS/NZS 4600) design rules are over-conservative. Young (2004, 2005) then proposed a new design rule for axially

loaded fixed ended CFS plain angle section columns. This was verified by Silvestre et al. (2012) when estimating the member capacity of columns, with more accurate results obtained. On the other hand, Shifferaw and Schafer (2011) found that fixed ended plain and lipped angles exhibited post-buckling strength. Rasmussen and Hancock (1994) studied the flexural buckling behavior of CFS channel section columns and showed that the Australia-New Zealand standard (AS/NZS 4600) design guidelines are conservative for intermediate and long columns under fixed ended condition.

There is limited research available on the axial capacity of CFS channels undergoing local-overall buckling interaction failure. The issue is addressed in the present paper, offering results of 40 experiments on CFS channel sections under axial compression. Prior to compression testing, the material properties and initial imperfections were measured for all test specimens. A non-linear FE model was also developed, which showed good agreement with the experimental test results, both in terms of failure modes and axial capacities. The validated FE model was then used to conduct a parametric study to determine the axial capacity of CFS channels, undergoing local-overall buckling interaction. Four different steel grades, two different cross sections and four different thicknesses were considered. The results obtained from the parametric study were compared against design strengths calculated using current guidelines AISI (2016), AS/NZS (2018), and Eurocode (2006). Having compared FE and test results against the design strengths calculated in accordance with the AISI (2016) and AS/NZS (2018), improved design rules are proposed in this study for predicting accurately the axial capacity of CFS channel section columns undergoing local-overall buckling interaction.

2 Current Design Guidelines

2.1 AISI (2016) Specification and AS/NZ Standard (2018)

The axial capacities obtained from the experiments (as described in Sect. 3) were compared against the un-factored design strengths calculated in accordance with the AISI (2016) and AS/NZS (2018) standards. It should be noted that design strengths calculated from both the AISI (2016) and AS/NZS (2018) depend on the effective area of the cross-sections. For channel sections, the un-factored design strength of axially loaded compression members can be calculated by the Equations given next.

$$P_{\text{AISI \& AS/NZS}} = A_e F_n \quad (1)$$

The critical buckling stress (F_n) can be calculated by using Eqs. (2) and (3), as given next.

$$\text{For, } \lambda_c \leq 1.5 : F_n = (0.658 \lambda_c^2) F_y \quad (2)$$

$$\text{For, } \lambda_c > 1.5, F_n = \left(\frac{0.877}{\lambda_c^2} \right) F_y \quad (3)$$

where A_e is the effective area of the section, F_n is the critical buckling stress, λ_c is the non-dimensional slenderness ratio.

The non-dimensional critical slenderness (λ_c) can be calculated by using Eq. (4) as given next.

$$\lambda_c = \sqrt{\frac{F_y}{F_n}} \quad (4)$$

where F_n is the least of the applicable elastic flexural, torsional, and flexural-torsional buckling stresses. Further details regarding the current design guidelines can be found in the AISI (2016) and AS/NZS (2018) standards.

2.2 Eurocode (EN 1993-1-3) (2006)

Design strength of axially loaded compression members calculated using the Eurocode (P_{EN}) depends on the effective area of the section. According to EC3 (BSEN1993-1-3) (2018), the axial strength (P_{EN}) is calculated as follows:

$$P_{\text{EN}} = \chi A_e F_y \quad (5)$$

where A_e is the effective area of the section. F_y is the yield stress. χ is the reduction factor for the relevant buckling mode

$$\chi = \frac{1}{\phi + \sqrt{\phi^2 - \bar{\lambda}^2}} \quad \text{but } \chi \leq 1.0 \quad (6)$$

$$\phi = 0.5 \left[1 + \alpha (\bar{\lambda} - 0.2) + \bar{\lambda}^2 \right] \quad (7)$$

$$\bar{\lambda} = \sqrt{\frac{A_e F_y}{N_{\text{cr}}}} = \frac{L_{\text{cr}}}{i} \frac{\sqrt{A_e/A_g}}{\lambda_1} \quad (8)$$

$$\lambda_1 = \pi \sqrt{\frac{E}{F_y}} \quad (9)$$

where L_{cr} is in plane buckling length, i is the radius of gyration for the particular axis, dependent on cross sectional properties. λ is the imperfection factor and N_{cr} is the elastic critical force, calculated by using cross sectional properties.

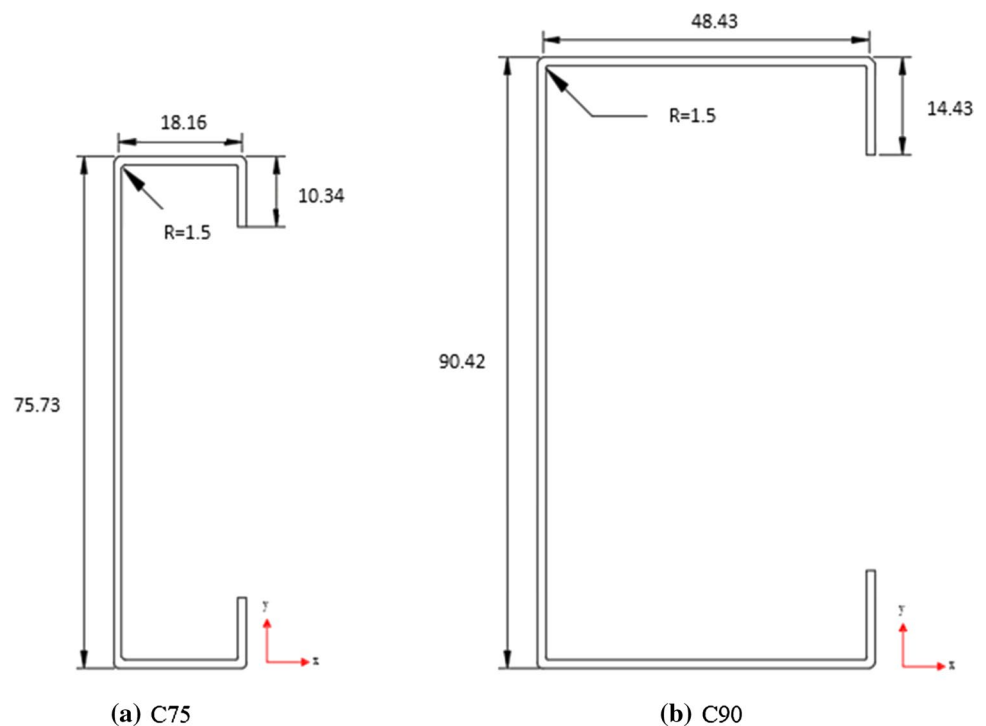
3 Experimental Investigation

3.1 Test Specimens

Figure 1 shows the details of the CFS channel sections considered in the experimental program. These are referred to as C75 and C90. The measured specimen dimensions are shown in Tables 1 and 2 for C75 and C90, respectively. In Tables 1 and 2, the overall web length of sections is defined by the notation “A”. The flange width and lip width of channel sections are defined by “B” and “C”, respectively. The length and thickness of channel sections are defined as “L” and “t”, respectively. The test program comprised 40 specimens; 20 each for C75 and C90 channel sections, subdivided into four different column heights: 300 mm, 500 mm, 1000 mm, and 2000 mm.

All columns were tested with pin-ended boundary conditions, apart from the 300 mm (stub) column which was tested as a fixed ended column. In Tables 1 and 2, the specimens have been sub-divided into stub (300 mm long), short (500 mm long), intermediate (1000 mm long) and slender (2000 mm long) columns for C75 and C90 sections, respectively. In the experimental program, five different nominal thicknesses were considered for all four heights: 1.2 mm, 1.5 mm, 2 mm, 2.5 mm, and 3 mm.

Fig. 1 Details of cold-formed steel channel columns investigated in this study



3.2 Determination of Material Properties

Tensile coupon tests were carried out to determine the material properties of the test specimens. The tensile coupons were cut from the center of the web plate in the longitudinal direction of the untested specimens. Five coupons were cut from the longitudinal direction of the coupons for each of the thicknesses for both the C75 and C90 channels. The tensile coupons were tested according to the British Standard for Testing and Materials for the tensile testing of metals BS EN (2001) using 12.5 mm wide coupons of a gauge length 50 mm. The coupons were tested in an MTS displacement-controlled testing machine using friction grips. Two strain gauges and a calibrated extensometer of 50 mm gauge length were used to measure the longitudinal strain. The average stress–strain curve of the steel used in this research is shown in Fig. 2a, b for full and initial curves, respectively. As can be seen from Fig. 2, the Young’s modulus and yield stress of the steel were 207 GPa and 560 N/mm², respectively. The average values of the material properties are also reported in Table 3.

3.3 Specimen Labelling

The test specimens were labelled such that the cross section of channel section, nominal length of specimen and specimen number were expressed by the label. Figure 3 shows an example of the specimen labelling used in this study. The channel sections are denoted by their web depth, i.e. 75 in the label (Fig. 3). The column length is stated at the end of

Table 1 Experimental test results: C75

Type	Specimen label	Web		Flange		Lip	Length	Thickness	Experimental results	AISI and AS/NZS Design strengths		Eurocode design strengths		FEA results		Proposed design strengths using Eq. (12)		Failure mode
		A	B	C	L					t	P_{EXP}	$P_{AISI&AS/NZS}$	$P_{AISI&AS/NZS}$	P_{EN}	P_{EXP}/P_{EN}	P_{FEA}	P_{EXP}/P_{FEA}	
Stub (300 mm)	C75-L300-1	73.7	19.6	10.3	271	1.21	60.6	58.3	1.04	57.4	1.06	61.2	0.99	-	-	-	Local	
	C75-L300-2	73.5	19.8	10.5	280	1.52	72.6	69.1	1.05	69.3	1.05	74.1	0.98	-	-	-	Local	
	C75-L300-3	72.4	19.6	10.8	276	2.02	92.6	87.4	1.06	83.9	1.10	91.7	1.01	-	-	-	Local	
	C75-L300-4	73.7	19.7	11.2	282	2.53	120.6	114.9	1.05	118.4	1.02	118.2	1.02	-	-	-	Local	
	C75-L300-5	73.6	19.7	10.9	284	3.02	156.9	152.3	1.03	146.4	1.07	152.2	1.03	-	-	-	Local	
	Mean	-	-	-	-	-	-	-	-	-	-	-	-	-	-	-	-	-
	COV	-	-	-	-	-	-	-	-	-	-	-	-	-	-	-	-	-
Short (500 mm)	C75-L500-1	73.6	19.5	10.2	689.0	1.19	42.0	41.2	1.02	40.1	1.05	40.8	1.03	-	-	-	Local	
	C75-L500-2	73.6	19.5	10.2	668.0	1.52	50.1	49.6	1.01	48.3	1.04	50.6	0.99	-	-	-	Local	
	C75-L500-3	73.6	19.6	10.3	670.0	2.01	75.9	73.7	1.03	70.7	1.07	74.4	1.02	-	-	-	Local	
	C75-L500-4	73.4	19.7	10.6	672.0	2.51	104.6	102.5	1.02	96.8	1.08	103.6	1.01	-	-	-	Local	
	C75-L500-5	73.6	19.7	10.5	678.0	3.01	131.8	126.7	1.04	117.7	1.12	131.8	1.00	-	-	-	Local	
	Mean	-	-	-	-	-	-	-	-	-	-	-	-	-	-	-	-	
	COV	-	-	-	-	-	-	-	-	-	-	-	-	-	-	-	-	
Intermediate (1000 mm)	C75-L1000-1	75.3	20.2	10.5	1133	1.22	22.0	20.0	1.10	18.6	0.98	23.4	0.94	21.6	1.02	-	Local + Overall	
	C75-L1000-2	75.4	19.8	10.6	1131	1.51	30.3	27.3	1.11	25.5	0.96	32.6	0.93	29.4	1.03	-	Local + Overall	
	C75-L1000-3	75.5	19.7	10.7	1133	2.00	44.6	41.0	1.09	38.9	0.97	47.4	0.94	43.7	1.02	-	Local + Overall	
	C75-L1000-4	75.8	19.8	10.7	1182	2.52	63.8	56.8	1.12	53.7	0.94	70.9	0.90	61.3	1.04	-	Local + Overall	
	C75-L1000-5	76.0	20.1	10.4	1131	3.00	81.7	71.9	1.14	67.1	0.95	91.8	0.89	79.3	1.03	-	Local + Overall	
	Mean	-	-	-	-	-	-	1.11	-	1.18	-	1.02	-	1.03	-	-	-	
	COV	-	-	-	-	-	-	0.02	-	0.03	-	0.01	-	0.01	-	-	-	
Slender (2000 mm)	C75-L2000-1	73.2	20.3	10.7	2184	1.23	4.6	4.1	1.11	3.9	0.95	4.9	0.93	4.4	1.04	-	Local + Overall	
	C75-L2000-2	73.6	20.2	10.6	2183	1.49	8.0	7.2	1.11	6.8	0.96	9.0	0.89	7.8	1.03	-	Local + Overall	
	C75-L2000-3	73.8	20.3	10.8	2184	1.99	16.6	14.6	1.14	13.5	0.96	18.4	0.90	16.3	1.02	-	Local + Overall	
	C75-L2000-4	73.9	20.2	10.8	2184	2.51	23.8	21.2	1.12	20.4	0.93	27.0	0.88	23.3	1.02	-	Local + Overall	
	C75-L2000-5	73.7	20.3	10.9	2183	3.02	34.6	30.8	1.12	28.6	0.95	38.4	0.90	33.6	1.03	-	Local + Overall	
	Mean	-	-	-	-	-	-	-	1.12	-	1.19	-	0.90	-	-	-	-	
	COV	-	-	-	-	-	-	-	0.01	-	0.03	-	0.02	-	-	-	-	

Table 2 Experimental test results: C90

Type	Specimen label	Web (mm)	Flange (mm)	Lip (mm)	Length (mm)	Thickness (mm)	Experimental Results	AISI and AS/NZS design Strengths		Eurocode design strengths		FEA results		Proposed design strengths using Eq. (12)		Failure mode	
								$P_{AISI&AS/NZS}$ (kN)	$P_{AISI&AS/NZS}^{EXP}$	P_{EN} (kN)	P_{EN}^{EXP}	P_{FEA} (kN)	P_{FEA}^{EXP}	$P_{AISI&AS/NZS}$ [using Eq. (12)]	$P_{AISI&AS/NZS}^{EXP}$ [using Eq. (12)]		
Stub(300 mm)	C90-L300-1	74.1	19.6	10.6	274	1.22	68.4	66.4	1.03	64.5	1.00	69.1	0.99	-	-	Local	
	C90-L300-2	74.3	19.5	10.2	281	1.51	80.4	78.8	1.02	71.4	1.06	82.0	0.98	-	-	Local	
	C90-L300-3	73.8	19.6	10.7	276	2.00	104.3	100.3	1.04	95.9	1.02	102.3	1.02	-	-	Local	
	C90-L300-4	74.6	19.7	10.2	268	2.50	133.6	129.7	1.03	127.2	0.99	128.5	1.04	-	-	Local	
	C90-L300-5	74.7	19.2	10.2	274	3.03	173.8	168.7	1.03	156.0	1.05	170.4	1.02	-	-	Local	
Short (500 mm)	Mean	-	-	-	-	-	-	-	1.03	-	1.02	-	1.01	-	-	-	-
	COV	-	-	-	-	-	-	-	0.01	-	0.03	-	0.02	-	-	-	-
	C90-L500-1	73.6	19.2	10.2	657	1.19	49.0	48.0	1.02	46.9	0.98	47.1	1.04	-	-	Local	
	C90-L500-2	73.7	19.3	10.6	681	1.48	61.1	59.9	1.02	53.2	1.03	59.9	1.02	-	-	Local	
	C90-L500-3	73.8	19.1	11.3	676	2.02	88.9	88.9	1.00	79.6	1.05	84.7	1.05	-	-	Local	
	C90-L500-4	73.8	19.6	11.4	681	2.50	116.6	117.8	0.99	104.6	1.05	114.3	1.02	-	-	Local	
	C90-L500-5	73.9	19.4	11.4	679	3.01	145.8	141.6	1.03	137.5	1.00	144.4	1.01	-	-	Local	
	Mean	-	-	-	-	-	-	-	-	1.01	-	1.02	-	1.03	-	-	-
	COV	-	-	-	-	-	-	-	-	0.02	-	0.03	-	0.02	-	-	-

Table 2 (continued)

Type	Specimen label	Web (mm)	Flange (mm)	Lip (mm)	Length (mm)	Thickness (mm)	Experimental Results	AISI and AS/NZS design Strengths		Eurocode design strengths		FEA results		Proposed design strengths using Eq. (12)		Failure mode
								$P_{AISI&AS/NZS}$	$P_{EXP}/P_{AISI&AS/NZS}$	P_{EN}	P_{EXP}/P_{EN}	P_{FEA}	P_{FEA}	$P_{AISI&AS/NZS}$ [using Eq.(12)]	$P_{EXP}/P_{AISI&AS/NZS}$ [using Eq. (12)]	
Intermediate (1000 mm)	C90-L1000-1	76.3	20.4	10.6	1140	1.20	26.7	24.0	1.23	21.9	1.22	25.9	1.03	25.7	1.04	Local + Overall
	C90-L1000-2	76.2	20.2	10.5	1142	1.51	36.3	32.3	1.27	29.8	1.22	35.2	1.03	35.2	1.03	Local + Overall
	C90-L1000-3	76.4	20.3	10.5	1139	2.02	54.0	47.0	1.32	43.1	1.25	53.5	1.01	51.4	1.05	Local + Overall
	C90-L1000-4	76.8	20.7	10.2	1137	2.52	78.4	69.8	1.26	65.5	1.20	76.9	1.02	76.9	1.02	Local + Overall
	C90-L1000-5	76.3	20.1	10.4	1144	3.01	90.0	81.9	1.21	79.3	1.13	91.8	0.98	87.4	1.03	Local + Overall
Slender (2000 mm)	Mean	-	-	-	-	-	-	-	1.26	-	1.20	-	1.01	-	1.03	-
	COV	-	-	-	-	-	-	-	0.04	-	0.04	-	0.02	-	0.01	-
	C90-L2000-1	75.2	20.6	10.8	2178	1.21	4.3	4.6	0.88	4.5	0.96	4.2	1.02	4.1	1.04	Overall
	C90-L2000-2	75.4	20.8	10.9	2170	1.51	7.4	7.6	0.95	7.5	0.98	7.2	1.02	7.2	1.03	Overall
	C90-L2000-3	75.5	20.9	10.7	2175	2.02	22.9	19.9	1.32	18.4	1.24	22.2	1.03	22.5	1.02	Local + Overall
	C90-L2000-4	74.6	20.2	10.7	2180	2.52	30.9	27.2	1.29	24.2	1.28	31.2	0.99	30.9	1.00	Local + Overall
	C90-L2000-5	74.1	20.5	10.8	2181	3.00	45.7	41.1	1.23	39.1	1.17	45.2	1.01	43.9	1.04	Local + Overall
	Mean	-	-	-	-	-	-	-	1.13	-	1.13	-	1.01	-	1.03	-
	COV	-	-	-	-	-	-	-	0.21	-	0.15	-	0.01	-	0.02	-

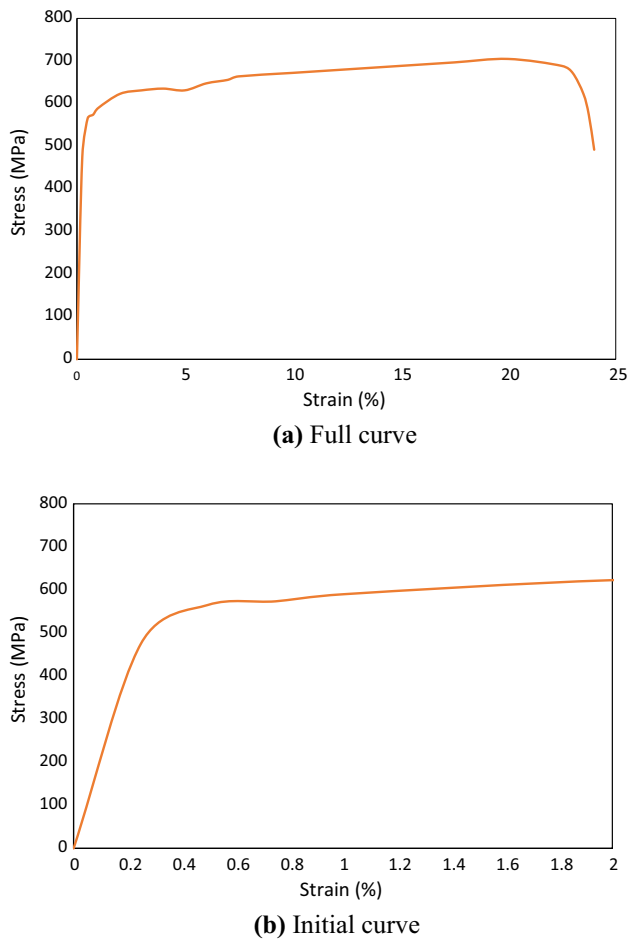


Fig. 2 Average stress–strain curves of CFS used in this research (average of C75 and C90 sections)

Table 3 Material properties obtained from the tensile coupon tests

Section	Gauge length	Gauge width	Ultimate stress	Yield stress	Young’s modulus
	L_0	b	σ_u	$\sigma_{0.2}$	E
	(mm)	(mm)	(MPa)	(MPa)	(GPa)
Average values from C75 and C90 sections	50	12.5	690	560	207



Fig. 3 Specimen labelling

the label as ‘L’. The number “1” at the end of the label refers to the specimen number.

3.4 Test-Rig and Testing Procedure

Figure 4 shows a photograph of the test set-up for stub (300 mm long) and intermediate (1000 mm long) columns. In order to record the axial load, the external load cell was positioned at the base of the columns. Two Linear Variable Displacement Transducers (LVDTs) were positioned at the web and a third LVDT was positioned at the top. LVDT positions are numbered as 1, 2 and 3, as shown in Fig. 4a for stub columns and 1, 2, 3,4 5 and 6 for intermediate column tests (Fig. 4b). The axial load was applied to the specimens via a 600 kN capacity GOTECH, GT-7001-LC60 Universal Testing Machine (UTM). The machine was displacement controlled and the loading rate was kept below 25 kg/cm²/s for all test specimens. The columns were centered and aligned so that the load could be applied through the centroid of the sections.

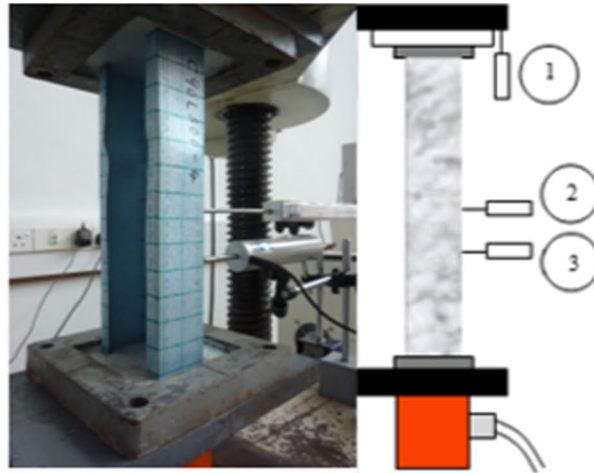
3.5 Measurement of Initial Imperfections

Figure 5a shows the set-up used to measure initial geometric imperfections for all test specimens. The test specimens were placed on a level surface with one end fixed using a G-clamp. A level was used to ensure surface integrity. A LVDT with an accuracy of 0.01 mm was used to record the readings at 20 mm along the length of the sections at the center of the web, flanges, and edge of the lips. Gridlines with 20 mm spacings were drawn on the outer surface of every test specimen to guide the movement of the LVDT along a straight line. The locations of LVDTs are shown in Fig. 5b. A typical plot of the measured initial imperfections versus the channel column length is shown in Fig. 5c for C75-L300-1. In Fig. 5d, another plot of initial imperfections versus the length is shown for C75-L2000-1. The highest imperfections of the investigation samples were 0.21 mm for a 300 mm long column, 0.24 mm for a 500 mm long column, 0.42 mm for a 1000 mm long column and 0.60 mm for a 2000 mm long column.

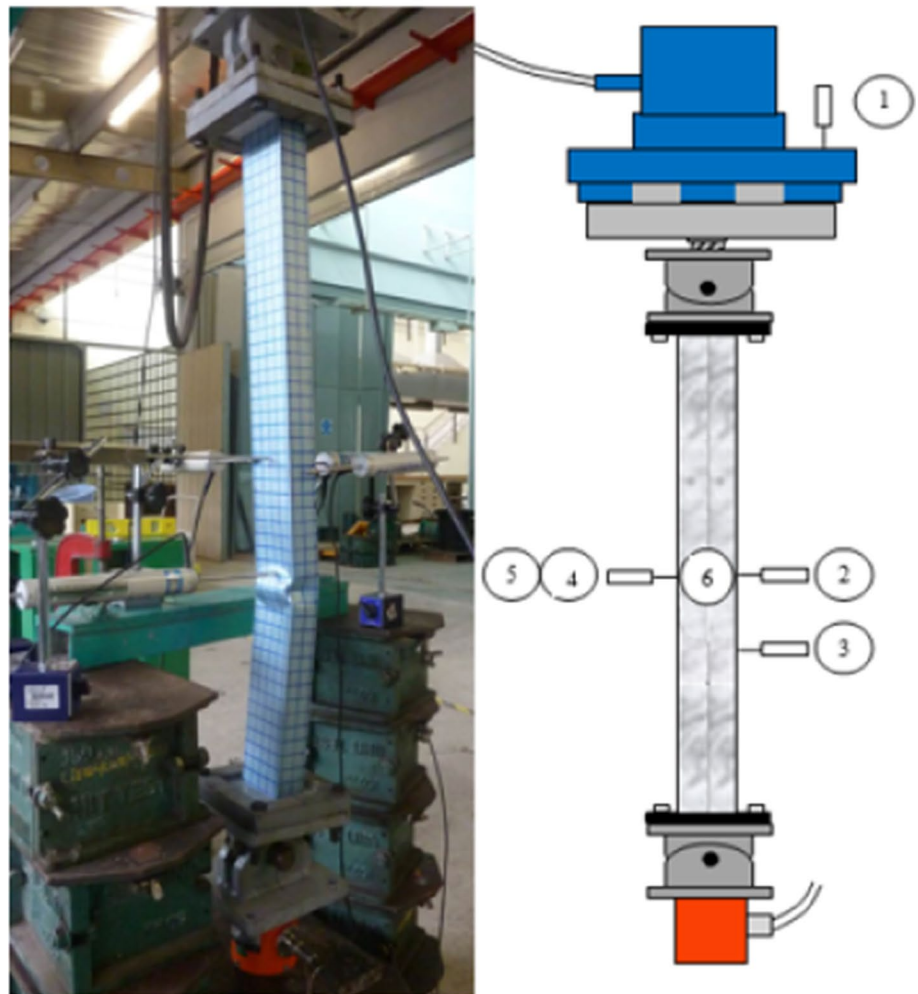
3.6 Experimental Results

The dimensions of test specimens and the experimental failure loads (P_{EXP}) are shown in Tables 1 and 2 for C75 and C90, respectively. Tables 1 and 2 also shows the axial capacity of channel sections calculated in accordance with the AISI (2016), AS/NZS (2018) and Eurocode (2006). The non-dimensional slenderness of the CFS channel sections were calculated and shown in Tables 1 and 2 for C75 and C90, respectively. As can be seen from Tables 1 and 2, the AISI (2016) and AS/NZS (2018) standards are conservative by around 10%

Fig. 4 Photograph of a test set-up

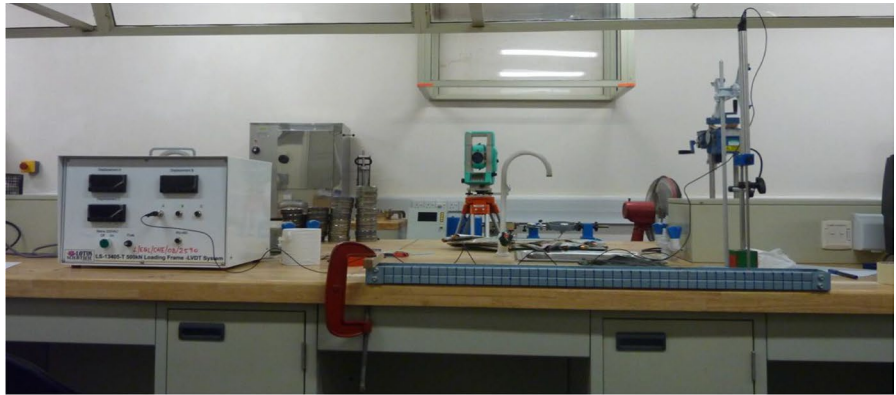


(a) Stub tests

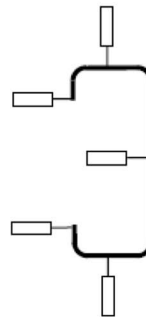


(b) Intermediate column tests

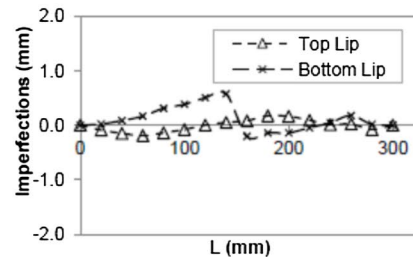
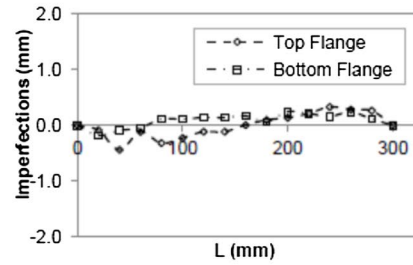
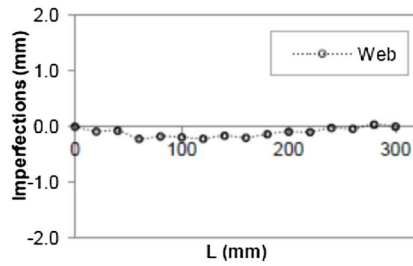
Fig. 5 Details of imperfection measurements



(a) Imperfection measurements setup

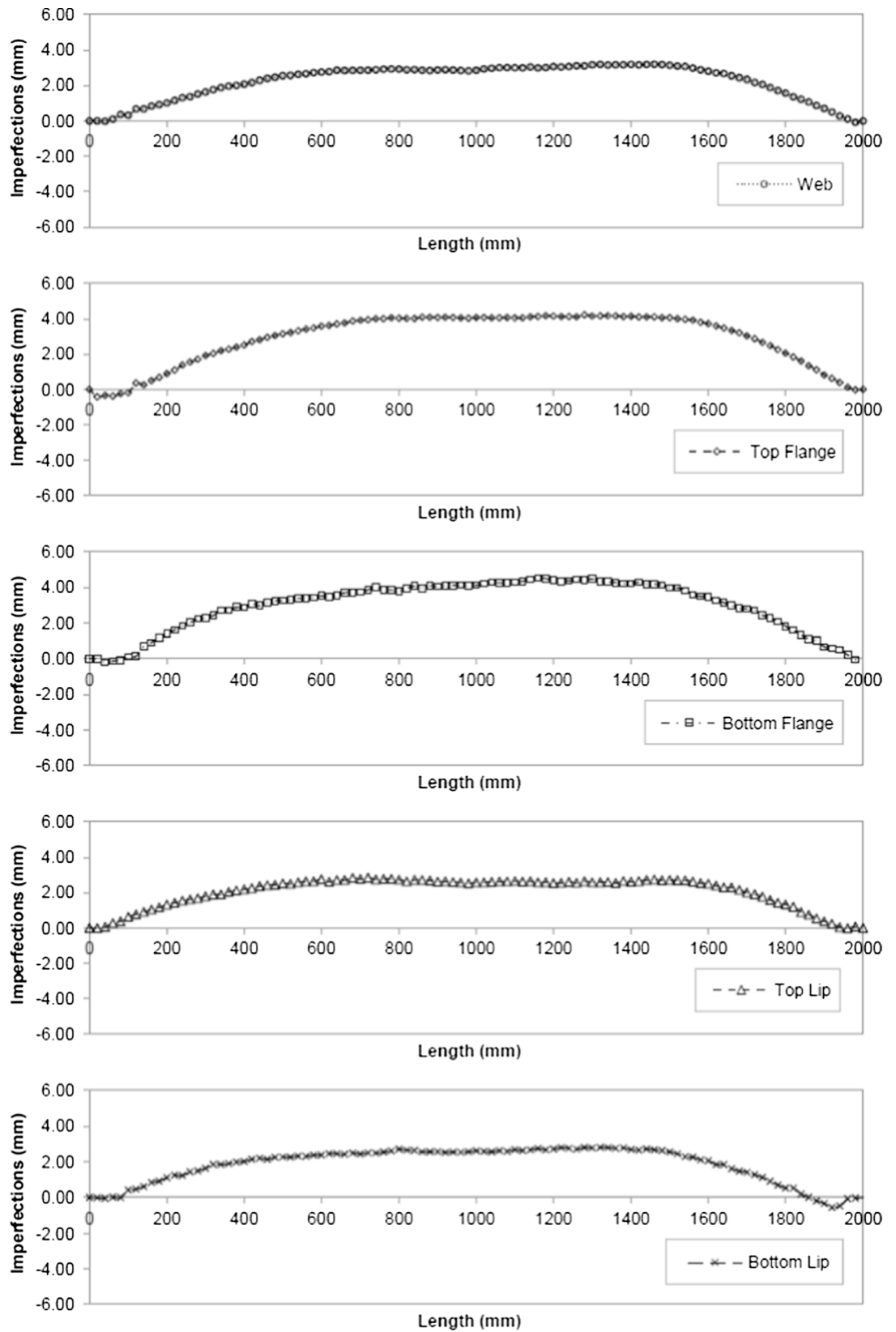


(b) Position of LVDTs to measure imperfections



(c) Imperfection Results for C75-L300-1

Fig. 5 (continued)



(d) Imperfection Results for C75-L2000-1

for columns which failed in local-overall buckling interaction. In contrast, Eurocode (2006) design rules lead to considerably more conservative predictions of the column axial load capacity of CFS channels. In almost all cases, the Eurocode (2006) predictions were lower than the actual strength values obtained from the experimental tests of CFS channels failed in local-overall buckling interactions (the average ratios of test results to predicted values were 1.20 and 1.15, for C75 and C90 columns).

Different failure modes were observed as the length of channel sections varied. Almost all stub and short columns of C75 and C90 channels failed by local buckling. Local-overall buckling interaction was observed for all slender columns except C90-L2000-1 and C90-L2000-2, which were failed only by overall buckling. For most of the slender columns, overall buckling was observed with a large curved deformation at the mid-height. However, after the ultimate load was reached, localized deformation was visible near the mid-height of the compression side of the test specimens.

4 Numerical Study

4.1 General

The FE program ABAQUS (2018) was used to develop a numerical model in order to evaluate the axial capacities of CFS channel columns. The FE model was analyzed via two steps. The first analysis step was to conduct a linear perturbation analysis (Eigen-value analysis) to obtain the buckling modes (Eigen-modes). The second analysis step was to perform a load–displacement analysis to obtain the axial capacities, using the “general-static” method.

4.2 Geometry and Material Properties

The full geometry of the CFS channel sections was modelled. The material non-linearity was incorporated in the FE model by specifying the ‘true’ values of stresses and strains. The ABAQUS (2018) classical metal plasticity model was adopted for the purposes both of validation and for the parametric study (described in Sect. 5 of this paper). In order to define the isotropic yielding and plastic hardening of the steel, the von Mises yield surface was used in the classical metal plasticity model. The material properties were taken from the results of the tensile coupon tests (described in Sect. 3.2 of this paper) and included in the FE models. As per the ABAQUS manual (2018), the engineering material curve was converted into a true material curve by using the following Equations:

$$\sigma_{\text{true}} = \sigma(1 + \varepsilon) \quad (10)$$

$$\varepsilon_{\text{true(pl)}} = \ln(1 + \varepsilon) - \frac{\sigma_{\text{true}}}{E} \quad (11)$$

where E is the Young’s modulus, σ_{true} is the true stress, σ_u is the tensile ultimate strength, and σ and ε are the engineering stress and strain, respectively in ABAQUS (2018). The modulus of elasticity was taken as 207 GPa, and the elastic Poisson’s ratio, ν , was assumed as 0.30. Plastic material properties of the CFS channels, used in the FE model are shown in Table 4.

4.3 Element Type and Finite Element Meshing

The channel sections were modelled using the linear 4-noded quadrilateral thick shell elements (S4R5). To choose the optimum size of the FE meshing, a mesh sensitivity study was completed. The mesh sensitivity analysis revealed that a mesh size of 5×5 mm is suitable, given consideration to both computation time and accuracy of the numerical results. Figure 6a shows a typical FE mesh for C75-L500-2.

4.4 Boundary Conditions and Load Application

The CFS channel section columns investigated in this study were pin-ended, other than the stub which was fixed–fixed. To simulate the upper and lower pin-ended supports, the displacements and rotations (boundary conditions) were assigned to the upper and lower ends of the CFS channel sections through reference points. The load was applied to the center of gravity (CG) of the cross-section with the help of reference points, as shown in Fig. 6b. The distance between two reference points were equal to the effective length of the CFS channel section columns between the two hinged supports. The displacement control was used to load the channels, following the general-static (*STATIC) method. The non-linear geometric parameters (*NLGEOM) were activated in the FE model to consider large displacements in the simulation.

4.5 Imperfection Modeling

Initial geometric imperfections were included in the FE model by conducting elastic buckling analysis to determine

Table 4 Plastic material properties used in the FE model

Yield stress (MPa)	Plastic strain
560.00	0.0000
570.00	1.3446
580.00	1.4731
590.00	1.7351
600.00	2.8572

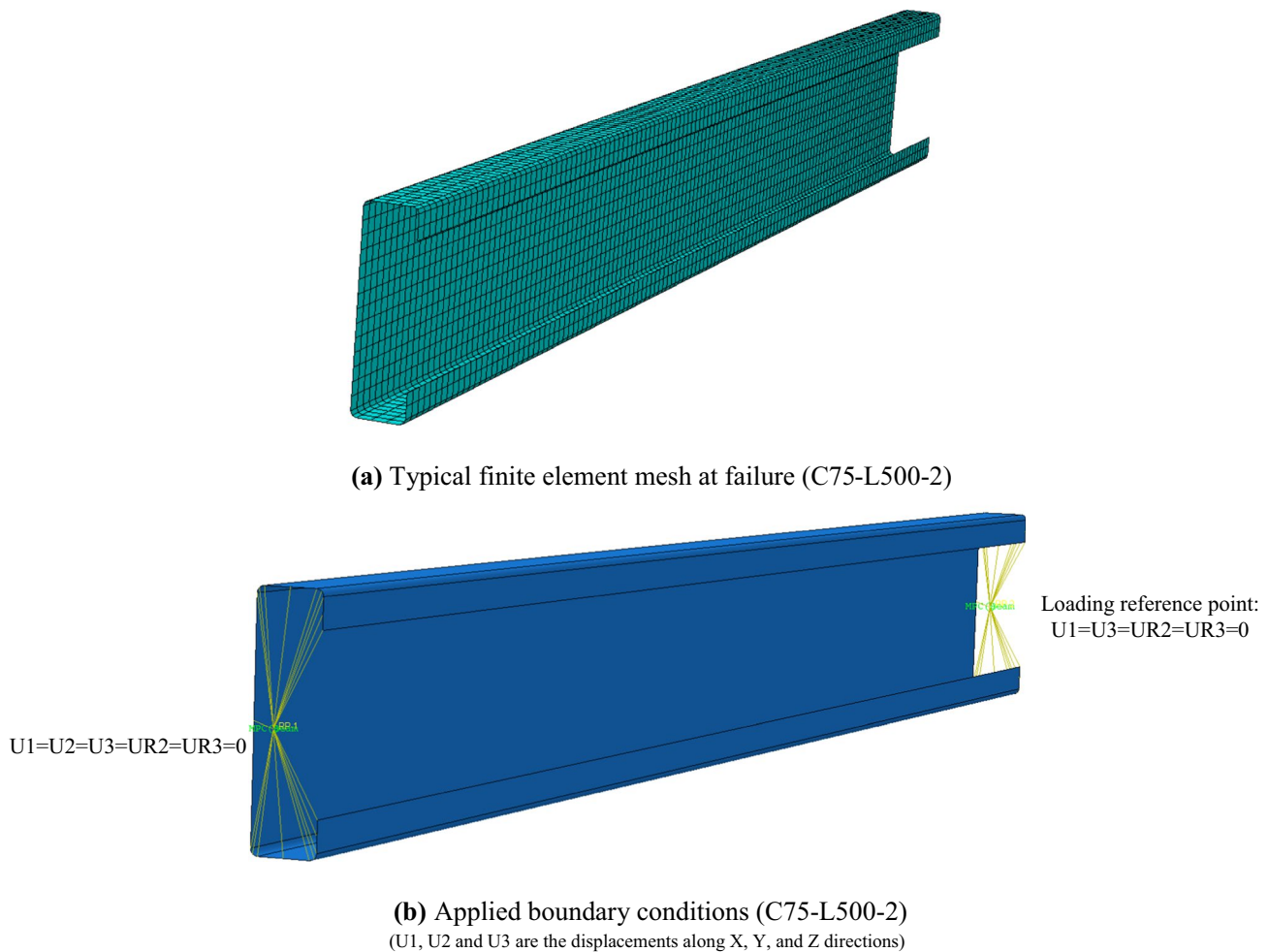


Fig. 6 Details of the finite element model developed for CFS channel column

the contours of such imperfect geometries. The scaled estimations of the general imperfections, as specified in Sect. 3.5 of this paper, were incorporated in the FE model. Moreover, the local imperfections having a magnitude of 0.5% of the channel thickness was used based on the recommendations of Ellobody and Young (2005). The same magnitude of local imperfections was also used by Roy et al. (2018) for modeling back-to-back built-up CFS channel sections under axial compression. The application of eigenvalue analysis enabled the achievement of overall and local buckling failure modes, as shown in Fig. 6c for C75L500-2.

4.6 Validation of the FE Model

The load–displacement behaviour obtained from the FE model are compared against the experimental failure load, as shown in Fig. 7a, b for specimens C75- L500-2 and C90-L500-2, respectively. Figure 8 shows the failure modes of stub, short, intermediate, and slender columns from both

the FE model and experiments. Tables 1 and 2 compare the experimental failure loads to the failure loads determined from the FE analysis for C75 and C90, respectively. As can be seen, the experimental and FE results show good agreement, both in terms of ultimate strength and failure modes.

5 Parametric Study

5.1 General

A parametric study, comprising 70 FE models, was conducted using the validated FE model. Both cross sections, i.e. C75 and C90, were considered in the parametric study (Fig. 1). The length of CFS channel sections was varied from 100 to 3000 mm (Tables 5, 6). Four different grades of steel were considered in the parametric study, i.e. G250, G450, G500, and G550. Also, four different thicknesses were considered: 0.95 mm, 1.20 mm, 2.20 mm and 2.40 mm.

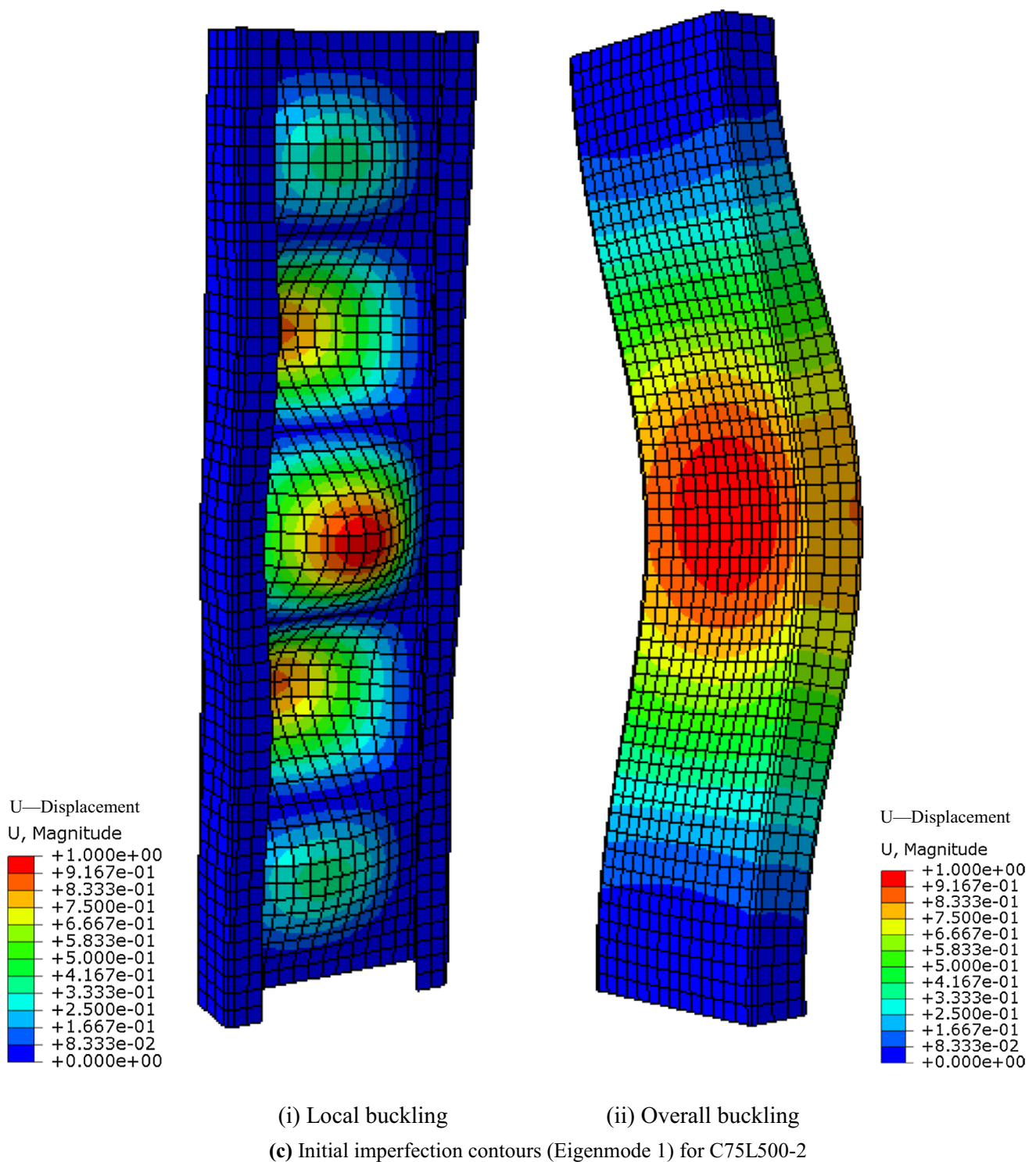


Fig. 6 (continued)

5.2 Parametric Study Results

In Tables 5 and 6, the FE strengths of the CFS channel sections obtained from the parametric study are shown. For comparison, the design strengths calculated in accordance

with the current AISI (2016) and AS/NZS (2018) are shown in Tables 5 and 6 for C75 and C90, respectively. As can be seen from both the Tables 5 and 6, the AISI (2016) and AS/NZS (2018) underestimates the axial capacity of CFS channel section columns by 10% on average for all channels

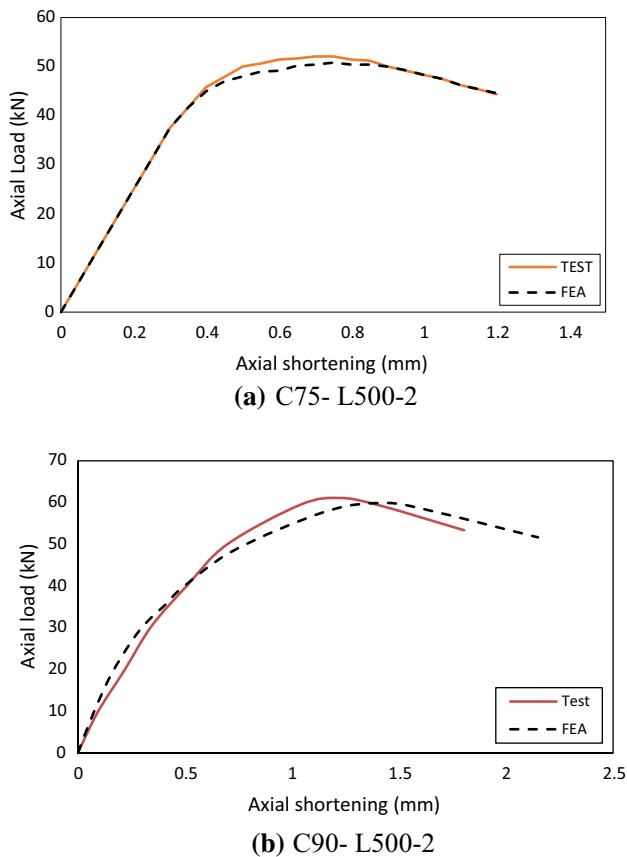


Fig. 7 Comparison of experimental failure load against the FEA results

which failed by local-overall buckling interaction. The comparison of experimental strengths against the design strengths calculated in accordance with the AISI (2016) and AS/NZS (2018) standards are also shown in Fig. 9a, b for C75 and C90, respectively. Tables 5 and 6 also show the comparison of FE strengths against the design strengths calculated from Eurocode (2006), which reveals that the Eurocode (2006) design strengths are considerably more conservative for determining the axial capacity of lipped channels failed in local-overall buckling interaction. The non-dimensional slenderness (λ_c) values reported in Tables 5 and 6 were calculated from Eqs. (2)–(4), found in current design codes, i.e. AISI (2016) and AS/NZS (2018) for CFS channel section columns.

6 Proposed Design Rules

There are mainly two regions in the design curve of AISI (2016) and AS/NZS (2018). The first region is for stub columns (where the non-dimensional slenderness ($\lambda_c \leq 1.5$)). The second region is for slender columns (where the non-dimensional slenderness ($\lambda_c > 1.5$)). These are defined by

Eqs. (2) and (3), respectively, as given in this paper. Tables 1 and 2 compare the experimental and FEA results with existing design equations for C75 and C90 columns, respectively. As can be seen from Tables 1 and 2, the AISI (2016) and AS/NZS (2018) is conservative by 10% on average for intermediate and slender columns which failed through local-overall buckling interaction. This highlights the need for improved design rules. The present paper proposes Eq. (12) for calculating the value of F_n when the non-dimensional slenderness (λ_c) is greater than 1.5. This is because the intermediate and slender columns are mainly susceptible to local-overall buckling interaction. For stub and short columns, the non-dimensional slenderness (λ_c) is less than or equal to 1.5, and the failure modes are mainly local or distortional buckling. Therefore, it is recommended to use the same equation of F_n as given in the AISI (2016) and AS/NZS (2018) [Eq. (2)], when the non-dimensional slenderness (λ_c) is less than or equal to 1.5.

$$\text{For, } \lambda_c > 1.5, F_n = \left(\frac{0.94}{\lambda_c^{1.92}} \right) F_y \quad (12)$$

As shown in Tables 1 and 2, the comparison of axial capacities from FEA and design strengths is calculated using Eq. (12) for C75 and C90, respectively. As can be seen from Tables 1 and 2, where design Eq. (12) was used, the design strengths are very close to the FE strengths.

7 Capacity Reduction Factor

The AISI standard (2016) recommends a statistical model to determine the capacity reduction factors. This model accounts for the variations in material, fabrication, and the loading effects. The capacity reduction factor ϕ is given by the following Equation:

$$\phi = 1.52 M_m F_m P_m e^{-\beta_0 \sqrt{V_m^2 + V_f^2 + C_p V_p^2 + V_q^2}} \quad (13)$$

where M_m and V_m are the mean and coefficient of variation of the material factor 1.1, 0.1; F_m , and V_f are the mean and coefficient of variation of the fabrication factor 1, 0.05; V_q is the coefficient of variation of load effect 0.21; β_0 is the target reliability index 2.5; C_p is the correction factor depending on the number of tests; P_m is the mean value of the tested to predicted load ratio; and V_p is the coefficient of variation of the tested to predicted load ratio. V_p and P_m values must be determined from experiments or analyses. In this investigation, ultimate loads obtained from FEA were considered. Hence V_p and P_m are the mean and coefficient of variation of the ratio of ultimate loads from FEA and design standards. The substitution of all the above values leads to the following Equation.

Fig. 8 CFS channels at failure

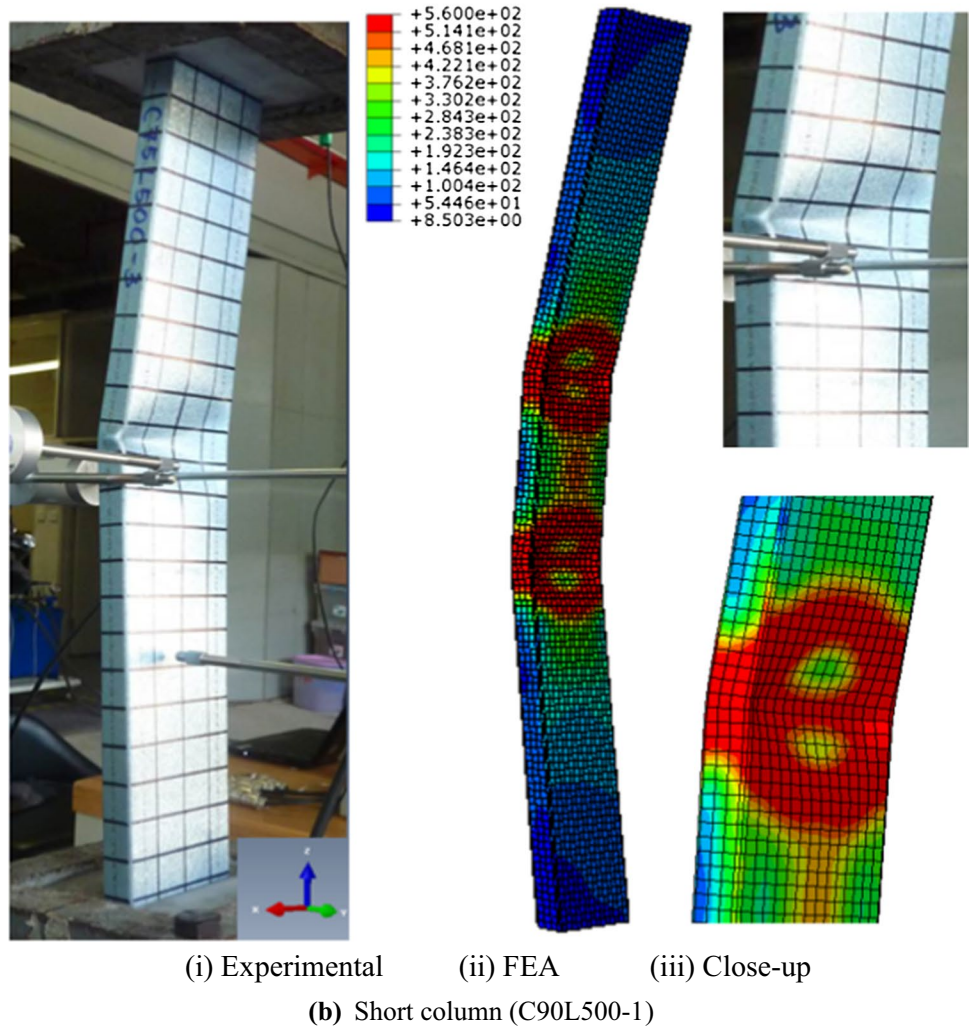
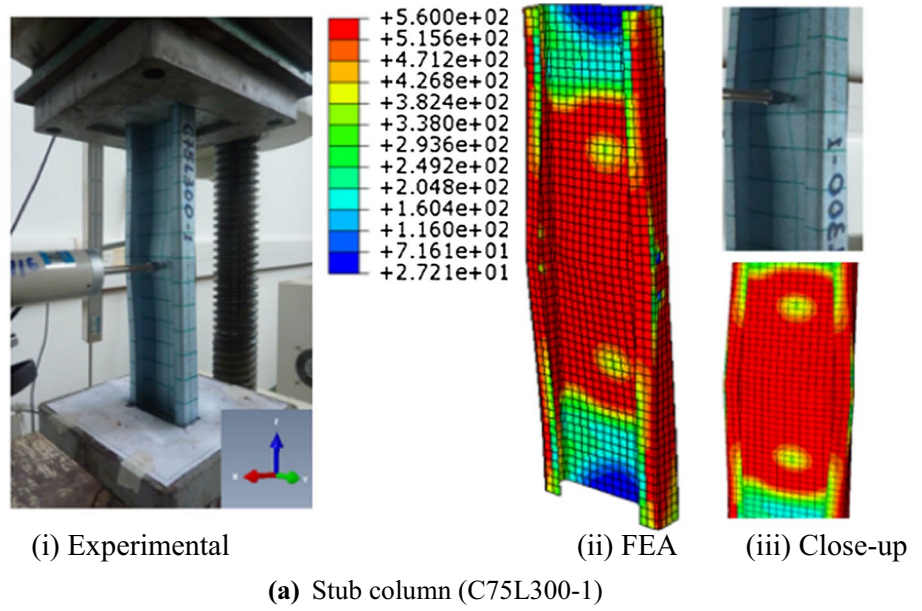
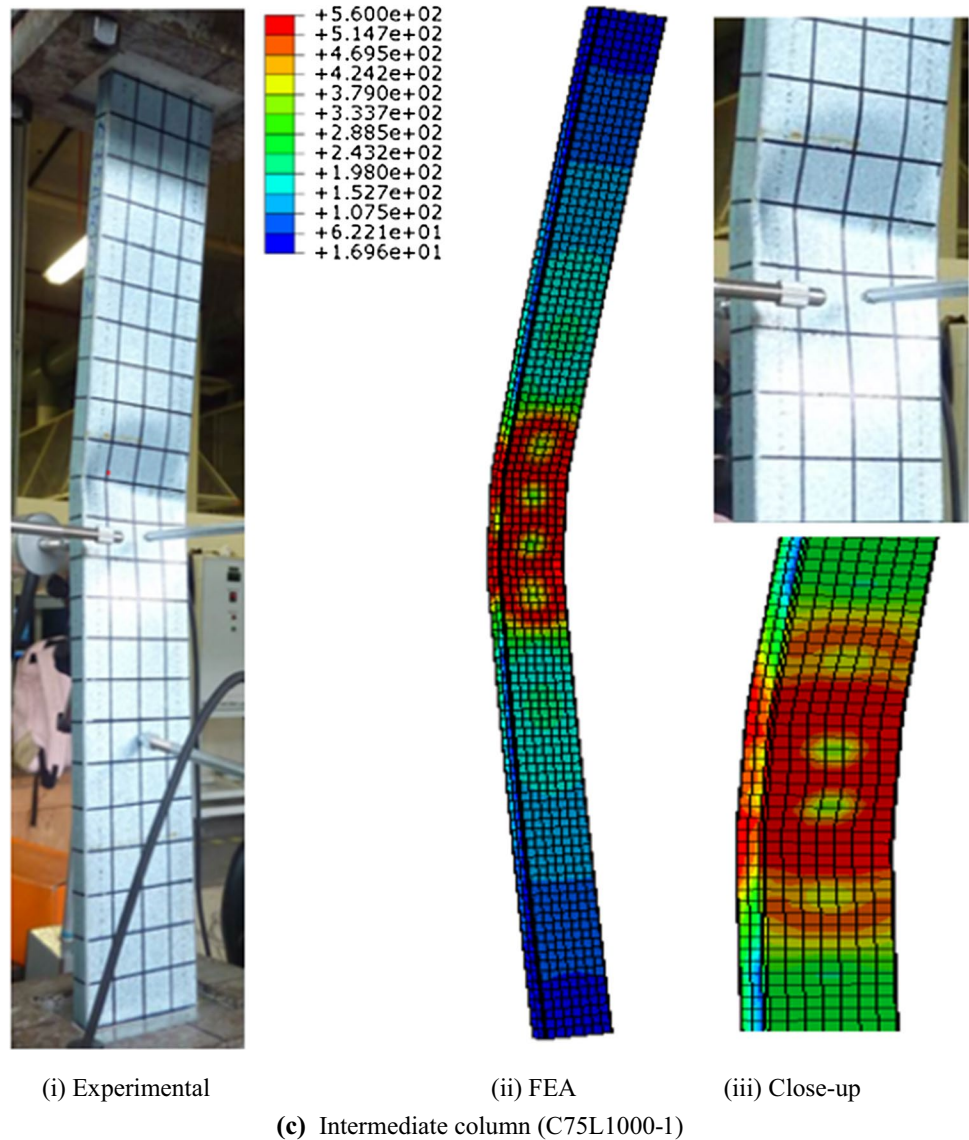


Fig. 8 (continued)



$$\phi = 1.615P_m e^{-2.5\sqrt{0.0566+C_p V_p^2}} \quad (14)$$

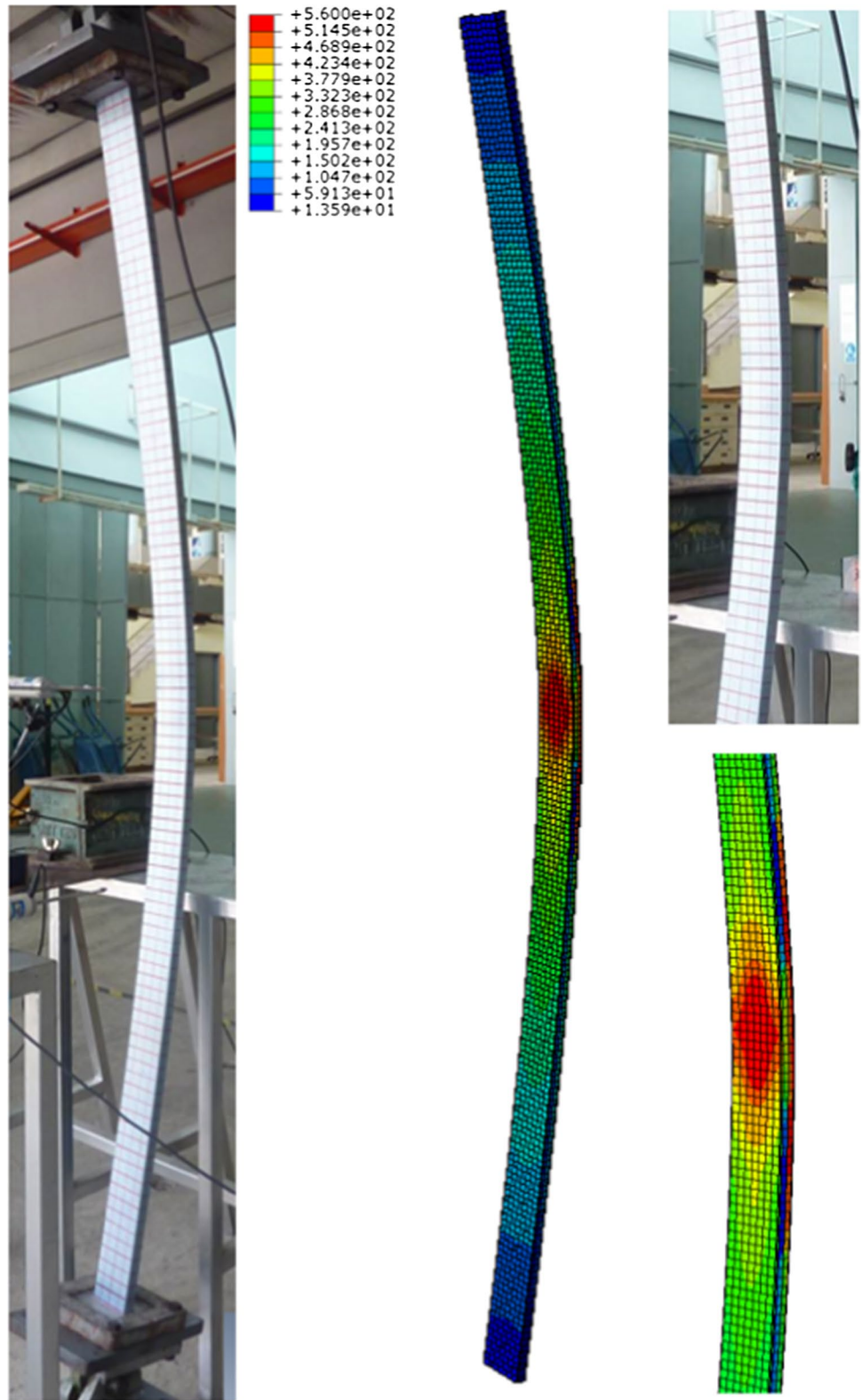
Equation (14) was used to determine the capacity reduction factors for the values obtained from the current AISI (2016) and AS/NZS (2018) and the proposed design rules. The AS/NZS (2018) recommends a capacity reduction factor of 0.85 for compression members. Tables 1 and 2 compare the test and FEA results with design strengths calculated from the existing design equations of AISI (2016) and AS/NZS (2018) and the proposed design equation [Eq. (7)]. The capacity reduction factor according to the current AISI (2016) and AS/NZS (2018), using Eq. (3) is 0.92, for CFS channel section columns undergoing local-overall buckling interaction. This slightly higher value of capacity reduction factor emphasizes the need of improved design rules. The capacity reduction factor is 0.86 when following proposed

design Eq. (12). Therefore, Eq. (7) is recommended instead of Eq. (3), for determining F_n , and calculating the axial capacity of CFS channel section columns undergoing local-overall buckling interaction.

8 Conclusions

This paper presents an experimental and finite element (FE) investigation to determine the axial capacity of CFS channel section columns subjected to local-overall buckling interaction. In total, 40 experimental tests on CFS channel section columns subjected to axial load were conducted and reported in this paper. Prior to the compression tests, initial imperfections were measured for all test specimens. The failure modes and deformed shapes of CFS channel section

Fig. 8 (continued)



(i) Experimental

(ii) FEA

(iii) Close-up

(d) Slender column (C75L2000-1)

Table 5 Comparison of axial capacities obtained from the FEA, AISI (2016), AS/NZS (2018) and Eurocode (2006): C75

Specimen	Section	Slenderness (λ_c)	Failure Mode(s)	P_{EN}	$P_{AISI\&AS/NZS}$	P_{FEA}	$\frac{P_{AISI\&AS/NZS}}{P_{FEA}}$	$\frac{P_{EN}}{P_{FEA}}$
	–	–	–	(kN)	(kN)	(kN)	–	–
G550×0.95×75×100	75×20×10	0.24	L	45.6	51.2	51.7	0.99	0.88
G550×0.95×75×300	75×20×10	0.52	L	41.5	46.1	48.0	0.96	0.86
G550×0.95×75×550	75×20×10	1.02	L	38.1	38.6	41.1	0.94	0.93
G550×0.95×75×1100	75×20×10	2.01	L+O	13.8	17.2	15.8	1.09	0.87
G550×0.95×75×1500	75×20×10	2.68	L+O	10.0	9.7	10.9	0.89	0.92
G550×0.95×75×2000	75×20×10	3.12	L+O	2.3	2.3	2.6	0.90	0.89
G550×0.95×75×3000	75×20×10	4.21	L+O	1.7	1.6	1.8	0.90	0.94
G250×0.95×75×100	75×20×10	0.18	L	32.4	35.2	34.9	1.01	0.93
G250×0.95×75×300	75×20×10	0.38	L	29.2	32.4	31.8	1.02	0.92
G250×0.95×75×550	75×20×10	0.74	L	26.4	29.6	30.2	0.98	0.87
G250×0.95×75×1100	75×20×10	1.47	L+O	17.3	16.8	18.3	0.92	0.95
G250×0.95×75×1500	75×20×10	1.96	L+O	9.0	9.4	10.3	0.91	0.87
G250×0.95×75×2000	75×20×10	2.28	L+O	2.1	2.2	2.4	0.90	0.86
G250×0.95×75×3000	75×20×10	3.07	O	1.5	1.5	1.7	0.89	0.89
G500×1.20×75×100	75×20×10	0.22	L	61.3	72.3	70.2	1.03	0.87
G500×1.20×75×300	75×20×10	0.48	L	54.7	63.2	62.0	1.02	0.88
G500×1.20×75×550	75×20×10	0.95	L	38.1	43.2	41.5	1.04	0.92
G500×1.20×75×1100	75×20×10	1.85	L+O	21.3	20.1	22.5	0.89	0.95
G500×1.20×75×1500	75×20×10	2.41	L+O	12.8	13.6	15.0	0.91	0.86
G500×1.20×75×2000	75×20×10	2.76	L+O	4.1	4.1	4.5	0.92	0.90
G500×1.20×75×3000	75×20×10	3.68	L+O	3.3	3.2	3.6	0.89	0.93
G250×2.40×75×100	75×20×10	0.12	L	84.8	89.8	88.9	1.01	0.95
G250×2.40×75×300	75×20×10	0.32	L	67.6	78.9	76.6	1.03	0.88
G250×2.40×75×550	75×20×10	0.65	L	47.2	55.8	55.2	1.01	0.86
G250×2.40×75×1100	75×20×10	1.20	L+O	36.5	35.5	39.8	0.89	0.92
G250×2.40×75×1500	75×20×10	1.44	L+O	29.1	29.7	32.7	0.91	0.89
G250×2.40×75×2000	75×20×10	1.59	O	9.2	9.7	10.8	0.90	0.86
G250×2.40×75×3000	75×20×10	2.26	L+O	6.5	6.7	7.5	0.89	0.86
G450×2.20×75×100	75×20×10	0.19	L	116.5	108.7	113.0	0.96	0.96
G450×2.20×75×300	75×20×10	0.45	L	95.7	94.0	94.9	0.99	0.95
G450×2.20×75×550	75×20×10	0.89	L	63.8	61.7	65.4	0.94	0.94
G450×2.20×75×1100	75×20×10	1.62	L+O	22.2	24.7	27.4	0.90	0.86
G450×2.20×75×1500	75×20×10	1.95	L+O	18.9	19.4	21.3	0.91	0.89
G450×2.20×75×2000	75×20×10	2.13	O	5.5	6.1	6.6	0.93	0.86
G450×2.20×75×3000	75×20×10	3.01	O	4.0	4.3	4.7	0.92	0.87

*Local = L, Overall = O

columns undergoing local-overall buckling interaction were discussed.

An elasto-plastic FE model was developed to include material non-linearity and geometric imperfections. The von Mises yield surface was defined in the classical metal plasticity model, which was adopted to incorporate isotropic yielding and plastic hardening of the steel. The FE model was validated against the test results. The validated FE model was then used to conduct an extensive parametric study (comprising 70 models) considering four different

steel grades and thicknesses, as well as two different cross-sections of CFS channels.

This study has also reviewed the accuracy of the current AISI (2016), AS/NZS (2018) and Eurocode (EN 1993-1-3) design guidelines for determining the axial capacity of CFS channel sections undergoing local-overall buckling interaction failure. The FE and experimental results were compared against the design strengths calculated in accordance with the AISI (2016) and AS/NZS (2018) and Eurocode (EN 1993-1-3). It was found that the

Table 6 Comparison of axial capacities obtained from the FEA, AISI (2016), AS/NZS (2018) and Eurocode (2006): C90

Specimen	Section	Slenderness (λ_c)	Failure Mode(s)	P_{EN} (kN)	$P_{AISI\&AS/NZS}$ (kN)	P_{FEA} (kN)	$\frac{P_{AISI\&AS/NZS}}{P_{FEA}}$	$\frac{P_{EN}}{P_{FEA}}$
	–	–	–				–	–
G550×0.95×90×1500	90×50×15	2.41	L+O	11.0	11.4	12.7	0.90	0.86
G550×0.95×90×1800	90×50×15	2.74	L+O	5.2	5.3	5.9	0.90	0.87
G550×0.95×90×2500	90×50×15	3.31	L+O	3.9	4.1	4.6	0.89	0.86
G550×0.95×90×3000	90×50×15	3.79	L+O	3.2	3.4	3.7	0.92	0.86
G550×0.95×90×3500	90×50×15	4.25	L+O	2.1	2.3	2.5	0.92	0.86
G550×0.95×90×4500	90×50×15	4.67	L+O	2.0	2.1	2.3	0.91	0.86
G550×0.95×90×6000	90×50×15	5.14	L+O	1.2	1.3	1.4	0.93	0.86
G250×0.95×90×1500	90×50×15	1.80	L+O	7.3	7.8	8.5	0.92	0.86
G250×0.95×90×1800	90×50×15	2.04	L+O	3.5	3.7	4.1	0.90	0.85
G250×0.95×90×2500	90×50×15	2.42	O	2.8	3.1	3.2	0.97	0.86
G250×0.95×90×3000	90×50×15	2.65	L+O	2.4	2.6	2.9	0.90	0.84
G250×0.95×90×3500	90×50×15	3.02	O	2.0	2.1	2.2	0.95	0.89
G250×0.95×90×4500	90×50×15	3.38	L+O	1.7	1.8	1.9	0.95	0.88
G250×0.95×90×6000	90×50×15	3.70	L+O	1.0	1.1	1.2	0.92	0.86
G500×1.20×90×1500	90×50×15	2.21	L+O	15.0	16.1	17.4	0.93	0.86
G500×1.20×90×1800	90×50×15	2.53	L+O	7.1	7.2	8.1	0.89	0.88
G500×1.20×90×2500	90×50×15	3.08	L+O	4.5	4.6	5.1	0.90	0.89
G500×1.20×90×3000	90×50×15	3.49	L+O	3.8	3.9	4.3	0.91	0.89
G500×1.20×90×3500	90×50×15	3.82	O	2.7	3.1	3.2	0.97	0.86
G500×1.20×90×4500	90×50×15	4.13	L+O	2.5	2.6	2.9	0.90	0.87
G500×1.20×90×6000	90×50×15	4.49	O	1.4	1.4	1.6	0.88	0.86
G250×2.40×90×1500	90×50×15	1.21	L+O	20.1	22.5	24.5	0.92	0.82
G250×2.40×90×1800	90×50×15	1.46	L+O	10.4	10.1	11.1	0.91	0.94
G250×2.40×90×2500	90×50×15	1.85	L+O	7.7	7.5	8.4	0.89	0.92
G250×2.40×90×3000	90×50×15	2.24	O	7.3	7.2	8.0	0.90	0.92
G250×2.40×90×3500	90×50×15	2.56	L+O	6.8	6.8	7.3	0.93	0.94
G250×2.40×90×4500	90×50×15	2.81	L+O	5.9	5.8	6.4	0.91	0.93
G250×2.40×90×6000	90×50×15	3.14	O	3.0	2.9	3.1	0.94	0.95
G450×2.20×90×1500	90×50×15	1.63	L+O	12.7	14.6	15.7	0.93	0.81
G450×2.20×90×1800	90×50×15	1.84	L+O	11.0	12.6	13.6	0.90	0.81
G450×2.20×90×2500	90×50×15	2.14	L+O	7.7	8.8	9.6	0.92	0.80
G450×2.20×90×3000	90×50×15	2.53	L+O	6.4	7.4	8.3	0.89	0.77
G450×2.20×90×3500	90×50×15	2.88	L+O	6.2	7.1	7.8	0.91	0.79
G450×2.20×90×4500	90×50×15	3.17	O	5.9	6.8	7.3	0.93	0.81
G450×2.20×90×6000	90×50×15	3.49	L+O	3.2	3.6	3.9	0.92	0.81

*Local=L, Overall=O

current design guidelines as per the AISI (2016) and AS/NZS (2018) standards underestimate the axial capacity by 10% on average for pin-ended CFS channel section columns undergoing local-overall buckling interaction. Eurocode (EN 1993-1-3) design rules lead to considerably more conservative predictions of the column axial

load capacity for CFS channels. This paper has, therefore, proposed modifications to the current design rules of AISI (2016) and AS/NZS (2018). The accuracy of proposed design rules was verified using the FE analysis and test results of CFS channel section columns undergoing local-overall buckling interaction.

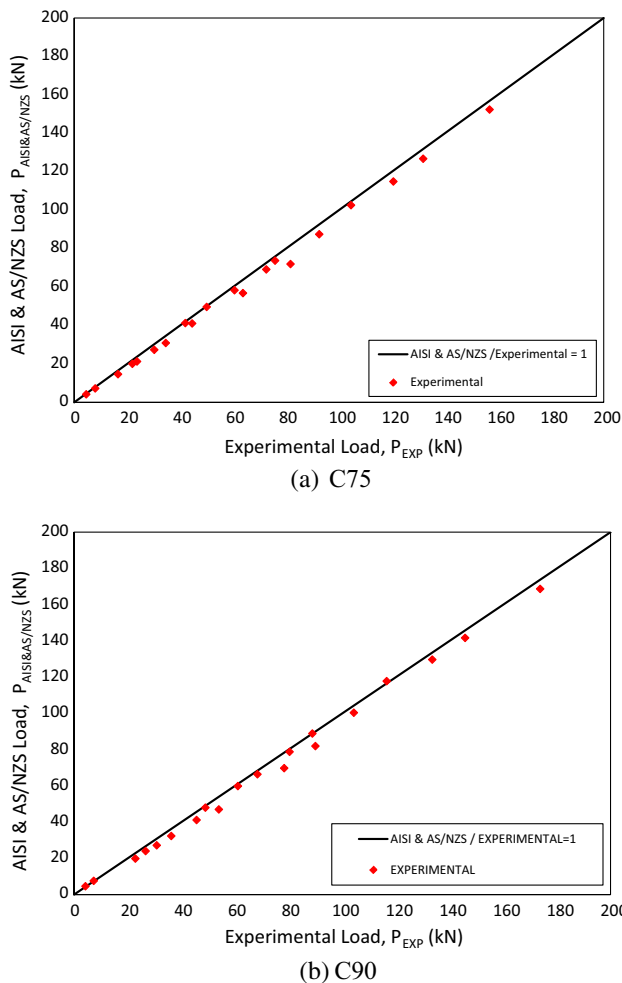


Fig. 9 Comparison of experimental strengths against the design strengths from current design guidelines [AISI (2016) and AS/NZS (2018) standards]

Acknowledgements The Ph.D. scholarship from Kiwi Steel NZ Ltd is greatly appreciated.

Funding This research did not receive any specific grants from funding agencies in the public, commercial, or not-for-profit sectors.

Compliance with ethical standards

Conflict of interest There is no conflict of interest between the authors or any third party regarding the publication of this article.

References

ABAQUS (2018) Version 6.14-2, USA: SIMULIA, Providence.
 AISI manual (2016). American Iron and Steel Institute: North American Specification for the Design of Cold-formed Steel Structural Members (NAS S100).

- AS/NZS 4600 (2018). Australia/New Zealand Standard: Cold-Formed Steel Structures, Standards Australia/Standards New Zealand.
- BS EN (2001) Tensile Testing of Metallic Materials Method of Test at Ambient Temperature, British Standards Institution.
- EC3. Eurocode 3 (2006) design of steel structures: Part 1–3: General rules: supplementary rules for cold-formed members and sheeting. BS EN 1993-1-3. Brussels: European Committee for Standardization.
- Ellobody, E., & Young, B. (2005). Behavior of cold-formed steel plain angle columns. *Journal of Structural Engineering*, 131, 457–466.
- Gunalan, S., & Mahendran, M. (2013). Improved design rules for fixed ended cold-formed steel columns subject to flexural-torsional buckling. *Thin-Walled Structure*, 73, 1–17.
- Hancock, G. J., Kwon, Y. B., & Bernard, E. S. (1994). Strength design curves for thin-walled sections undergoing distortional buckling. *Journal of Constructional Steel Research*, 31(2–3), 169–186.
- Heva, Y. B., & Mahendran, M. (2012). Flexural–torsional buckling tests of cold-formed steel compression members at elevated temperatures. *Steel and Comp Structure*, 14, 205–227.
- Kandasamy, R., Thenmozhi, R., & Jeyagopal, L. S. (2016). Flexural-torsional buckling tests of cold-formed lipped channel beams under restrained boundary conditions. *The International Journal of Steel Structures*, 16, 765–776.
- Loughlan, J., & Yidris, N. (2014). The local-overall flexural interaction of fixed-ended plain channel columns and the influence on the behaviour of local conditions at the constituent plate ends. *Thin Walled Structure*, 81, 132–137.
- Martins, A. D., Camotim, D., Dinis, P. B., & Young, B. (2015). Local-distortional interaction in cold-formed steel columns: mechanics, testing, numerical simulation, and design. *Structure*, 4, 38–57.
- Popovic, D., Hancock, G. J., & Rasmussen, K. J. R. (1999). Axial compression tests of cold-formed angles. *Journal of the Structural Engineering. American Society of Civil Engineers*, 125, 515–523.
- Rasmussen, K. J. R., & Hancock, G. J. (1994). Design of thin-walled plain channel section columns against flexural buckling. *Thin-Walled Structure*, 20, 219–240.
- Rhodes, J. & Harvery, J.M. (1977) Interaction behavior of plain channel columns under concentric or eccentric loading. In: Proceedings of the second international colloquium on the stability of steel structures. Liege, pp. 439–444.
- Roy, K., Ting, T. C. H., Lau, H. H., & Lim, J. B. P. (2018). Effect of thickness on the behavior of axially loaded back-to-back cold-formed steel built-up channel sections-Experimental and numerical investigation. *Structure*, 16, 327–346.
- Santos, D. E. S., Batisa, E. M., & Camotim, D. (2012). Experimental investigation concerning lipped channel columns undergoing local-distortional-global buckling mode interaction. *Thin-Walled Structure*, 54, 19–34.
- Shifferaw, Y. & Schafer, B.W. (2011). Behavior and design of cold-formed steel lipped and plain angles. In: Proceedings of the Structural Stability Research Council (SSRC) Annual Stability Conference, Pittsburgh, USA, pp. 10–14.
- Silvestre, N., Dinis, P. B., & Camotim, D. P. B. (2012). Developments on the design of cold-formed steel angles. *Journal of the Structural Engineering. American Society of Civil Engineers*, 139, 680–694.
- Wang, C. A., Zhang, Z. N., Zhao, D. Q., & Liu, Q. Q. (2016). Compression tests and numerical analysis of web-stiffened channels with complex edge stiffeners. *Journal of Constructional Steel Res.*, 116, 29–39.
- Ye, J., Hajirasouliha, I., & Becque, J. (2018). Experimental investigation of local-flexural interactive buckling of cold-formed steel channel columns. *Thin-Walled Structure*, 125, 245–258.

- Young, B. (2004). Tests and design of fixed-ended cold-formed steel plain angle columns. *Journal of the Structural Engineering. American Society of Civil Engineers*, 130, 1931–1940.
- Young, B. (2005). Experimental investigation of cold-formed steel lipped angle concentrically loaded compression members. *Journal of the Structural Engineering. American Society of Civil Engineers*, 131, 1390–1396.
- Young, B., & Hancock, G. J. (2003). Compression tests of channels with inclined simple edge stiffeners. *Journal of Structural Engineering ASCE*, 129, 1403–1411.
- Young, B. (2006). Local buckling and shift of effective centroid of slender sections. In: Proceedings of the advanced facade engineering and technology symposium, Hong Kong, China, pp. 119–132.
- Zhang, Y., Wang, C., & Zhang, Z. (2007). Tests and finite element analysis of pin-ended channel columns with inclined simple edge stiffeners. *Journal of Constructional Steel Res.*, 63, 383–395.

Publisher's Note Springer Nature remains neutral with regard to jurisdictional claims in published maps and institutional affiliations.